Supplementary Material

Additional information on the following is included:
1.The spectral method.
2.The lowest 100 singlet states with VEE and oscillator strengths, using the aug-ccpVTZ basis set and the B3LYP functional of DFT.
3.MP4(SDQ) equilibrium structures (X^1A' = -270.7956841 a.u.).
4. The X^1A' and $^2A'$ state modes used in the Franck-Condon analyses of the X^2A' ionic state and applied to the 3s-Rydberg state.
5.The VUV spectrum accompanied by 150 singlet state TDDFT calculations, using the Rydberg enhanced version of the aug-cc-pVTZ basis set. The original set shown in Figure 9 are in red; the s- and p-Rydberg functions lead to the combined valence and Rydberg state calculations in blue and green respectively. In most states, the original red series have been overlaid by the s- and p-Rydberg state energies and oscillator strengths. For example, the single green band at 4.5 eV has all three series of calculations overlaid with the p-set on top. In some cases, small shifts are observed as in the 5.5 to 6.0 eV region. Very small differences are seen in the very intense peak at 7.1 eV, where all three colours are apparent.
6. Harmonic frequencies (cm^{-1}) for the lowest singlet state (S_1) in C_S symmetry.
7.The planar forms of the HOMO and LUMO.
8. Asymmetric gaussian fit to the onset of the VUV spectrum.
9.Processing of regular residuals after fitting the onset to an asymmetric Gaussian function.
10. The full range of regular residuals after subtraction from the VUV spectral range.

SM1. The spectral method. Raw data for the energy region 5.2 to 5.85 eV (212 to 237 nm).

In order to show that the low cross-section fine structure observed in the VUV photoabsorption spectrum of CHT (those shown in figure 4 of the paper) are real absorption features and not an experimental artefact, we present here the raw data as measured on the AU-UV beam line during the investigation. The following procedure is carried out when measurements are made. The whole photoabsorption spectrum is measured in small sections, in order that an appropriate pressure of sample gas can be chosen, depending on the local cross-section. For each region, an I(o) scan is first measured with the cell evacuated. The signal recorded from the photomultiplier tube (PMT) is a measure of the light intensity passing through the cell, with a measurement time of ~2 seconds per wavelength step. The sample gas is then filled into the cell and two I(t) scans of the attenuated light are measured. The gas is pumped out again and a second I(o) is measured. This is repeated for each region of the spectrum measured. In Figure SM1.1 below the raw data measured over two regions which cover the range 5.2 to 5.85 eV, where fine structure is observed, are shown.

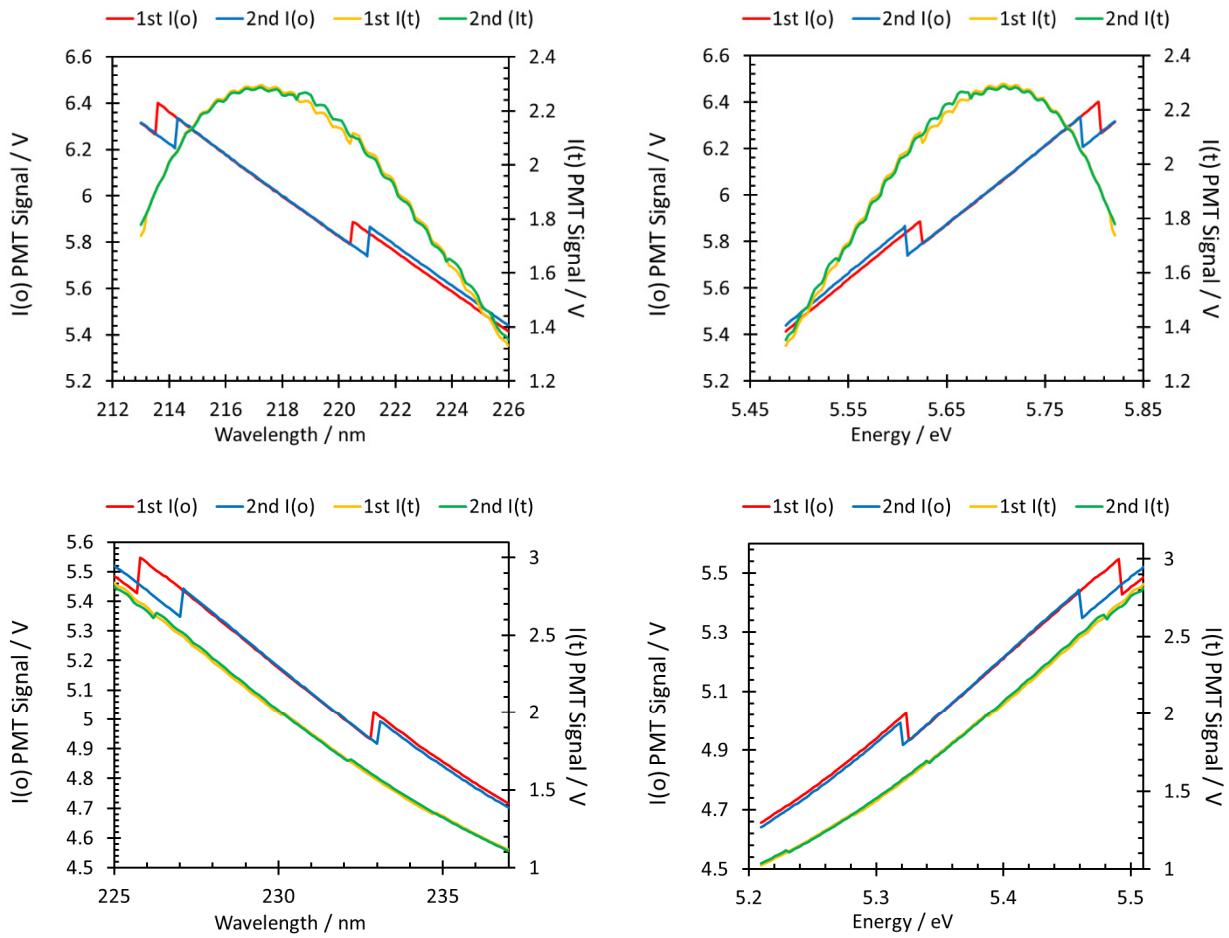

Figure SM1.1: Raw data measured for I(o) (red and blue curves) and I(t) (yellow and green curves) for (*top, left and right*) the region 212-226 nm (5.49 -5.85 eV) and (*bottom, left and right*) the region 225-237 nm (5.23-5.51 eV)

The synchrotron light source ASTRID2 operates in top-up mode in order to maintain a quasi-constant beam current and the steps observed in the raw data in Figure SM1.2 represent the occasional injection of electrons in order to maintain the beam current. Data collection is paused for several seconds before and after each injection in order to avoid measurement at the point of injection.

The beam current in ASTRID2 is simultaneously measured with the measured light intensity, and the data used for final calculation of the cross-sections is normalised to the changing beam current in order to remove these steps, shown in figure SXX below.

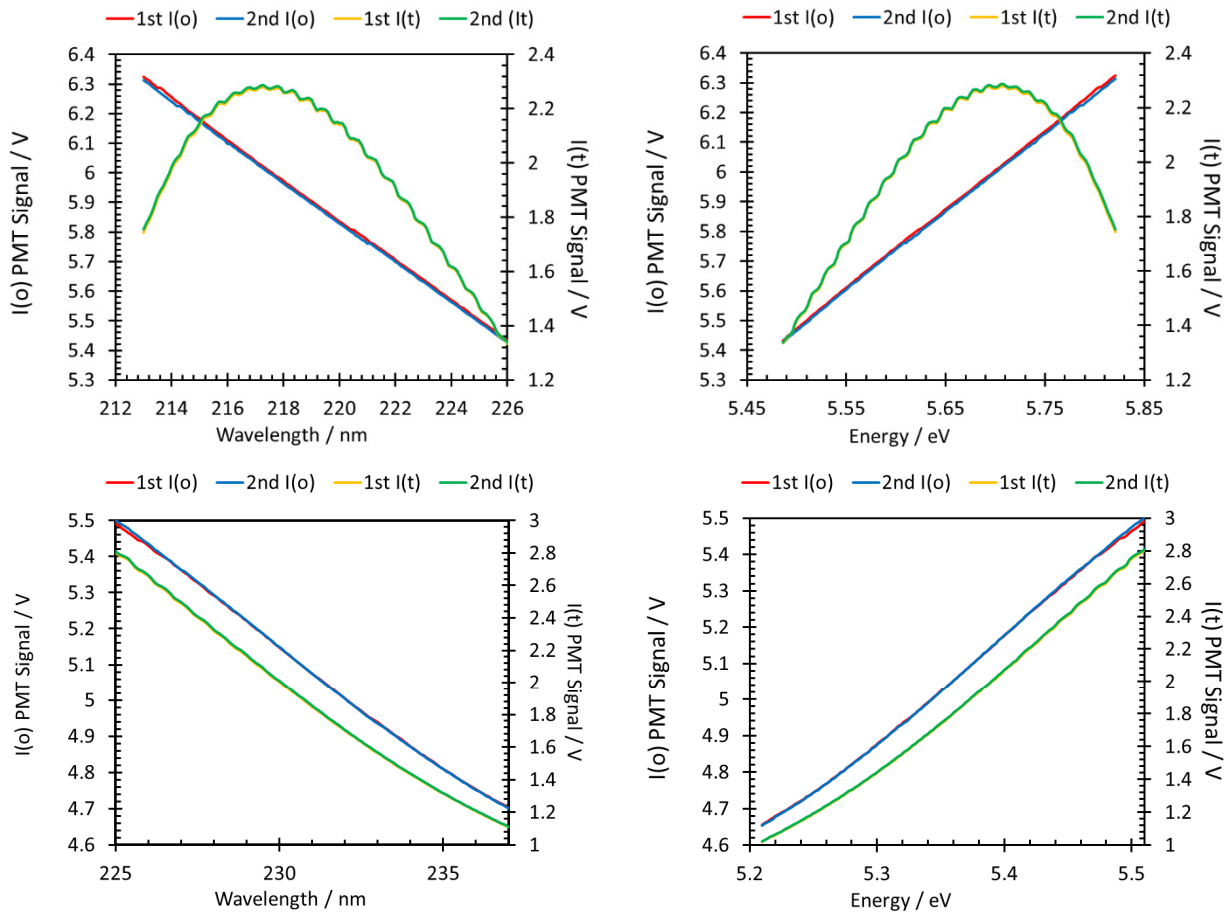

Figure SM1.2: Detector signals normalised to the measured ASTRID2 beam current for I(o) (red and blue curves) and I(t) (yellow and green curves) for (*top*, *left and right*) the region 212-226 nm (5.49 -5.85 eV)and (*bottom, left and right*) the region 225-237 nm (5.23-5.51 eV)

The data clearly shows that the features observed in the final spectrum are indeed due to absorption by the gas in the cell and not an experimental artefact. The features seen in the I(t) scans are not reproduced in the I(o) and the noise level in these scans is significantly lower than the variations in intensity observed due to absorption. The features are reproduced well in both I(t) scans and also observed for different loads of the gas cell with the sample when moving to a different section of the spectrum.

SM2. The lowest 100 singlet states with VEE and oscillator strengths, using the aug-cc-pVTZ basis set and the B3LYP functional of DFT.

Symmetry	Energy / eV	Oscillator strength	Symmetry	Energy / eV	Oscillator strength
A"	4.5086	0.0800	A'	9.2035	0.0073
A'	5.6745	0.0365	A"	9.2226	0.0260
A'	5.9050	0.0294	A'	9.2401	0.0231
A"	6.2490	0.0099	A"	9.2748	0.0181
A'	6.2923	0.0971	A'	9.2865	0.0078

A"	6.3026	0.0040	A"	9.3100	0.0505
A'	6.4025	0.1751	A'	9.3297	0.0061
A"	6.6745	0.0338	A"	9.3560	0.0069
A'	6.6802	0.0364	A"	9.4216	0.0222
A"	6.7443	0.0123	A'	9.4236	0.0053
A"	6.8786	0.0349	A'	9.4580	0.0301
A'	7.0587	0.1595	A'	9.5101	0.0189
A"	7.2847	0.0183	A"	9.5209	0.0542
A'	7.3240	0.0046	A'	9.5230	0.0206
A"	7.3914	0.0134	A"	9.6148	0.0042
A"	7.5024	0.0227	A'	9.6312	0.0076
A'	7.5810	0.0248	A"	9.6411	0.0127
A'	7.5970	0.0112	A'	9.6704	0.0100
A"	7.6542	0.0639	A"	9.7056	0.0102
A'	7.6835	0.0107	A'	9.7241	0.0092
A"	7.7045	0.0722	A'	9.9460	0.0154
A"	7.7493	0.0187	A"	9.9552	0.0041
A'	7.8061	0.0156	A'	9.9588	0.0205
A"	7.8557	0.0206	A'	9.9766	0.0044
A'	7.8606	0.0085	A'	10.0132	0.0046
A'	7.9537	0.0051	A'	10.0954	0.0190
A'	8.0232	0.0391	A"	10.1497	0.0091
A"	8.1359	0.0158	A'	10.1575	0.0156
A'	8.1560	0.0054	A'	10.3025	0.0335
A"	8.2601	0.0106	A'	10.3051	0.0323
A'	8.2898	0.0220	A"	10.3435	0.0142
A"	8.2997	0.0066	A'	10.3655	0.0232
A'	8.3810	0.0346	A'	10.4059	0.0268
A"	8.4937	0.0098	A'	10.4268	0.0048
A'	8.5375	0.0079	A"	10.4297	0.0045
A"	8.5594	0.0041	A'	10.4578	0.0078
A'	8.6158	0.0413	A"	10.4646	0.0057
A"	8.6371	0.0064	A'	10.5222	0.0107
A"	8.6724	0.0059	A"	10.5360	0.0044
A'	8.7014	0.0079	A"	10.5729	0.0046
A"	8.7196	0.0057	A"	10.6132	0.0059
A'	8.7236	0.0109	A'	10.6254	0.0095
A"	8.7659	0.0286	A"	10.6416	0.0261
A'	8.7897	0.0107	A"	10.6694	0.0316
A'	8.8038	0.0296	A'	10.7200	0.0420
A'	8.8859	0.0328	A"	10.7213	0.0059
A"	8.9924	0.0100	A'	10.7681	0.0430
A'	9.1160	0.0262	A'	10.7981	0.0286
A'	9.1446	0.0075	A'	10.8176	0.0312

SM3 MP4(SDQ) equilibrium structures (X^1A' = -270.7956841 a.u.)

State	Open shells	MP4SDQ/ a.u	DeltaE / eV
$1^3A''$	$10a'11a''$	-270.711527	2.2900
6	0.21744	1.63756	0
1	1.27368	1.96492	0
1	-0.34905	2.57675	0

6	-0.0622	-1.47885	0.73159
6	-0.0622	-1.47885	-0.73159
6	-0.0622	-0.42071	1.58678
6	-0.0622	-0.42071	-1.58678
6	-0.01882	0.95415	-1.30557
6	-0.01882	0.95415	1.30557
1	-0.09933	-2.46346	1.18283
1	-0.09933	-2.46346	-1.18283
1	-0.11885	-0.66895	2.64205
1	-0.11885	-0.66895	-2.64205
1	-0.03714	1.62137	-2.1595
1	-0.03714	1.62137	2.1595
Rotational constants (GHZ):	3.5509012	3.5470992	1.7998291
$^{3}A^{//}$	$14A^{/}11A^{//}$	-270.6242602	4.6646
6	0.53507	1.46839	0
1	1.53713	1.02918	0
1	0.63002	2.55348	0
6	0.15058	-1.45089	0.69019
6	0.15058	-1.45089	-0.69019
6	-0.2269	-0.36475	1.54959
6	-0.2269	-0.36475	-1.54959
6	-0.2269	0.99983	-1.213
6	-0.2269	0.99983	1.213
1	0.43761	-2.371	1.18659
1	0.43761	-2.371	-1.18659
1	-0.45324	-0.63156	2.57984
1	-0.45324	-0.63156	-2.57984
1	-0.85388	1.7009	-1.74565
1	-0.85388	1.7009	1.74565
Rotational constants (GHZ):	3.6550446	3.5925125	1.9745295
$^{3}A^{/}$	$11a^{/}12a^{/}$	-270.6174607	4.8496
6	0.24245	1.53651	0
1	1.35108	1.37646	0
1	0.09582	2.61694	0
6	0.44896	-1.36545	0.68196
6	0.44896	-1.36545	-0.68196
6	-0.31853	-0.45142	1.50279
6	-0.31853	-0.45142	-1.50279
6	-0.31853	0.93989	-1.24196
6	-0.31853	0.93989	1.24196
1	0.99549	-2.16308	1.18229
1	0.99549	-2.16308	-1.18229
1	-0.69659	-0.80309	2.45387
1	-0.69659	-0.80309	-2.45387
1	-0.6211	1.62187	-2.02761
1	-0.6211	1.62187	2.02761
Rotational constants (GHZ):	3.6361584	3.6097349	2.0033765

$^2A^{//}$	TZVP+B3LYP	-271.5970206	
6	4E-6	-1.68827	0
1	-0.86653	-2.37799	0
1	0.86654	-2.37799	0
6	-1E-6	1.52407	0.6985
6	-1E-6	1.52407	-0.6985
6	-1E-6	0.40429	1.56919
6	-1E-6	0.40429	-1.56919
6	0	-0.94685	-1.31391
6	0	-0.94685	1.31391
1	-2E-6	2.49751	1.1858
1	-2E-6	2.49751	-1.1858
1	-2E-6	0.66174	2.6302
1	-2E-6	0.66174	-2.6302
1	-1E-6	-1.60552	-2.18202
1	-1E-6	-1.60552	2.18202
Rotational constants (GHZ):	3.6065530	3.4397400	1.7793496
$^1A^{//}$	TDDFT+B3LYP	-271.470654543	
6	0	1.61589	0
6	0	0.95914	1.30457
6	0	-0.4103	1.58875
6	-1E-6	-1.49895	0.71024
6	-1E-6	-1.49895	-0.71024
6	0	-0.4103	-1.58875
6	0	0.95914	-1.30457
1	1E-6	1.63981	2.15003
1	1E-6	1.63981	-2.15003
1	1E-6	-0.6637	2.64535
1	1E-6	-0.6637	-2.64535
1	-1E-6	-2.47961	1.17552
1	-1E-6	-2.47961	-1.17552
1	0.83804	2.35653	0
1	-0.83805	2.35653	0
Rotational constants (GHZ):	3.5803160	3.5426498	1.7986346

SM4. Table SM4. The $X^1A^{/}$ and $^2A^{/}$ state modes used in the Franck-Condon analyses of the $X^2A^{/}$ ionic state and applied to the 3s-Rydberg state.

	$X^1A^{/}$ state			**$^2A^{/}$ state**		
Mode	Harmonic Frequency / cm^{-1}	Anharmonic Frequency / cm^{-1}	Difference / cm^{-1}	Harmonic Frequency / cm^{-1}	Anharmonic Frequency / cm^{-1}	Difference / cm^{-1}
1	3160	3023	-137	3240	3096	-144
2	3149	3013	-136	3227	3036	-192
3	3128	2945	-183	3217	3001	-216
4	3086	2955	-131	3141	2746	-395
5	2991	2819	-172	2940	2753	-187

6	1671	1635	-35	1671	1605	-67
7	1572	1527	-45	1608	1550	-58
8	1481	1436	-45	1495	1451	-44
9	1426	1395	-31	1442	1378	-63
10	1248	1231	-17	1318	1299	-20
11	1222	1204	-18	1265	1229	-36
12	1041	1018	-22	1092	1025	-67
13	977	961	-17	977	939	-38
14	939	921	-18	959	929	-31
15	921	904	-17	933	881	-52
16	812	802	-10	830	791	-39
17	726	712	-13	792	782	-10
18	668	661	-7	643	616	-27
19	432	429	-3	404	406	2
20	356	353	-4	367	355	-12
21	214	209	-5	88	85	-2
22	3155	3018	-126	3239	3055	-126
23	3134	2933	-171	3219	2995	-171
24	3122	2968	-133	3211	3023	-133
25	1663	1619	-45	1572	1523	-45
26	1477	1445	-35	1527	1488	-35
27	1387	1357	-32	1457	1420	-32
28	1327	1298	-49	1441	1310	-49
29	1269	1238	-22	1300	1251	-22
30	1211	1192	-47	1245	1172	-47
31	1068	1048	-22	1152	1110	-22
32	1000	981	-16	1036	1025	-16
33	983	964	-26	1008	988	-26
34	960	939	-16	943	919	-16
35	891	878	-28	876	848	-28
36	761	748	-11	783	783	-11
37	611	601	-15	483	495	-15
38	418	414	-4	419	421	-4
39	295	289	-6	222	214	-6

SM5. 5.The VUV spectrum accompanied by 150 singlet state TDDFT calculations, using the Rydberg enhanced version of the aug-cc-pVTZ basis set. The original set shown in Figure 9 are in red; the s- and p-Rydberg functions lead to the combined valence and Rydberg state calculations in blue and green respectively. In most states, the original red series have been overlaid by the s- and p-Rydberg state energies and oscillator strengths. For example, the single green band at 4.5 eV has all three series of calculations overlaid with the p-set on top. In some cases, small shifts are observed as in the 5.5 to 6.0 eV region. Very small differences are seen in the very intense peak at 7.1 eV, where all three colours are apparent.

SM5. The VUV spectrum accompanied by 150 singlet state TDDFT calculations, using the Rydberg enhanced version of the aug-cc-pVTZ basis set. The original set shown in Figure 9 are in red; the s- and p-Rydberg functions lead to the combined valence and Rydberg state calculations in blue and green respectively. In most states, the original red series have been overlaid by the s- and p-Rydberg state energies and oscillator strengths. For example, the single green band at 4.5 eV has all three series of calculations overlaid with the p-set on top. In some cases, small shifts are apparent as in the 5.5 to 6.0 eV region. Very small differences are apparent in the very intense peak at 7.1 eV, where all three colours are apparent.

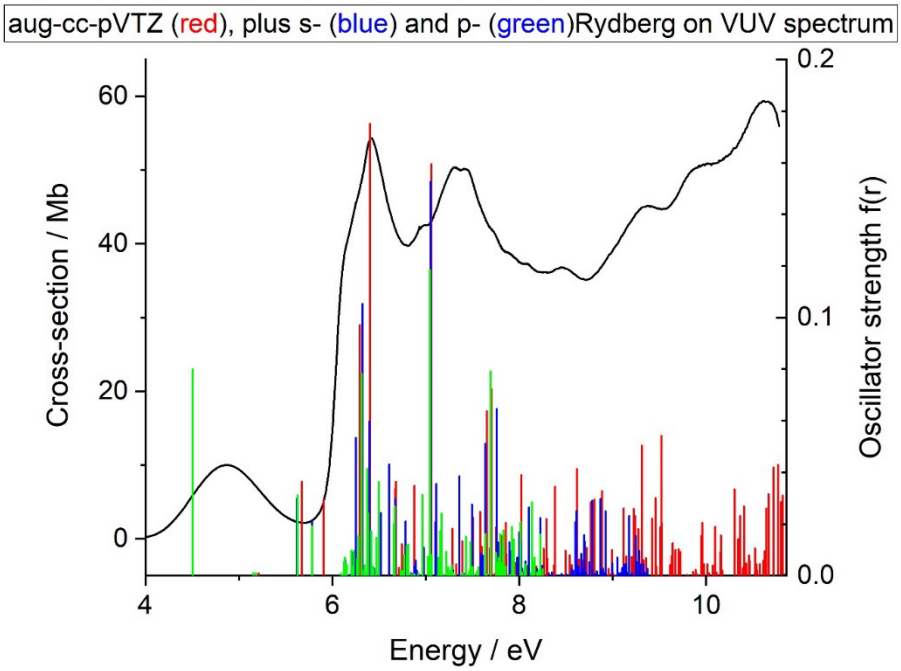

SM6. Table SM-VI. Harmonic frequencies (cm^{-1}) for the lowest singlet state (S_1) in C_S symmetry.

75	a/
381	a/
449	a/
684	a/
777	a/
833	a/
929	a/
958	a/
974	a/
1058	a/
1261	a/
1382	a/
1449	a/
1584	a/
1651	a/
1728	a/
3030	a/

3045	a/
1728	a/
3030	a/
3045	a/
3323	a/
3341	a/
173	a//
432	a//
569	a//
706	a//
936	a//
972	a//
995	a//
1050	a//
1198	a//
1214	a//
1332	a//
1459	a//
1536	a//
1597	a//
1675	a//
3329	a//

SM7. The planar forms of the HOMO and LUMO

MO26* a_2*

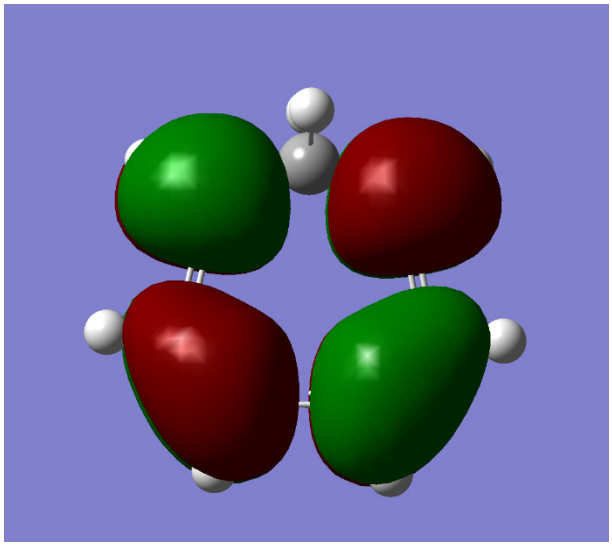

MO25 b_1

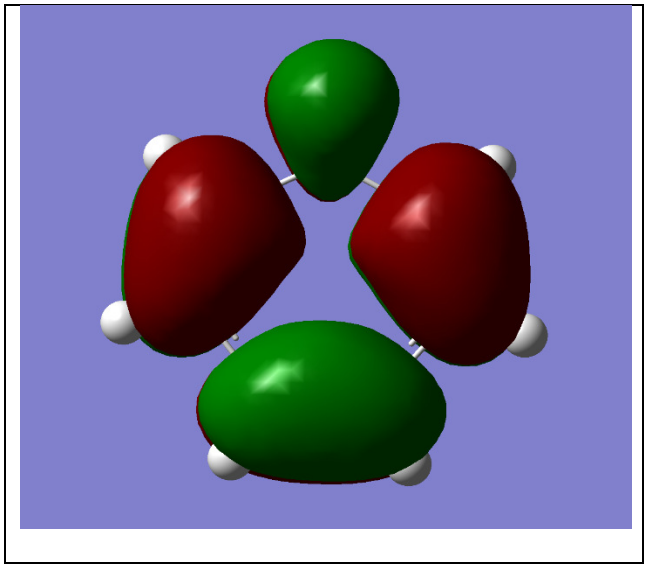

SM8. Asymmetric gaussian fit to the onset of the VUV spectrum

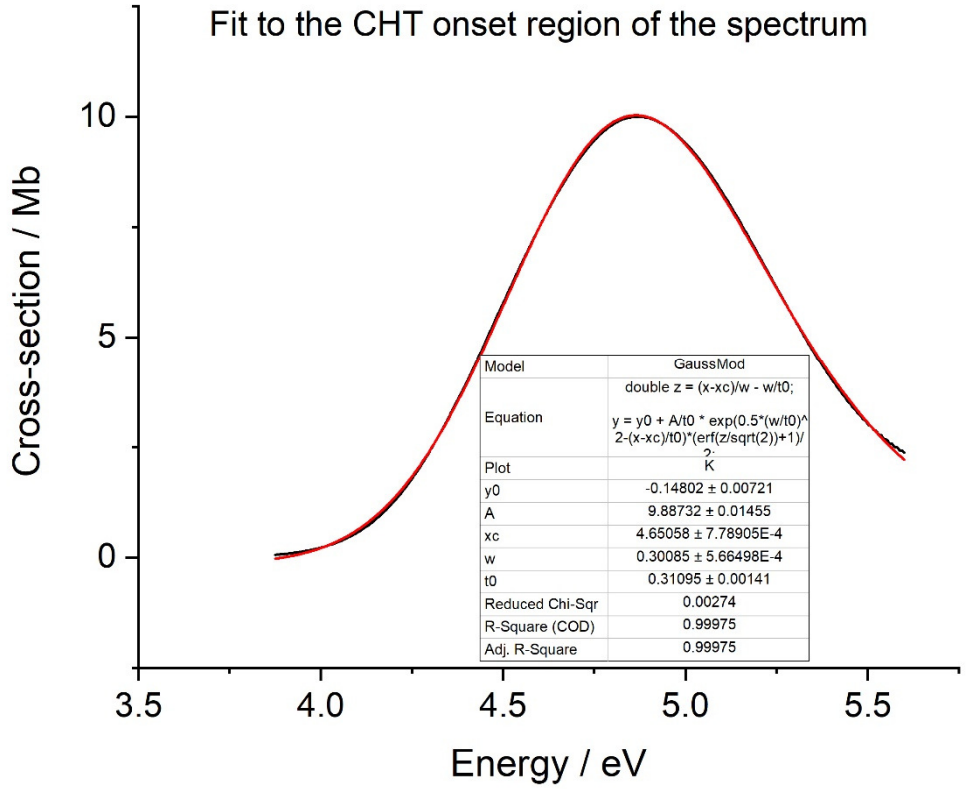

SM9. Processing of regular residuals after fitting the onset to an asymmetric Gaussian function.

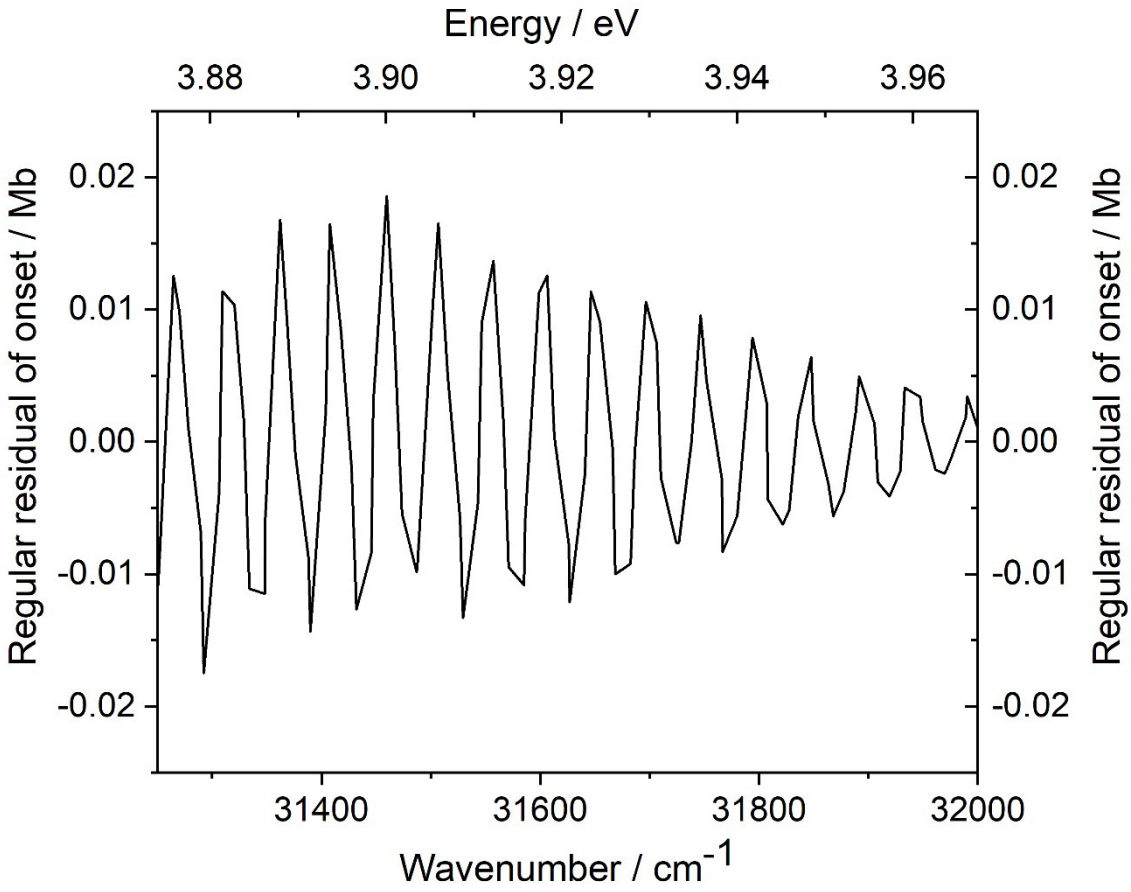

SM10. The full range of regular residuals after subtraction from the VUV spectral range.

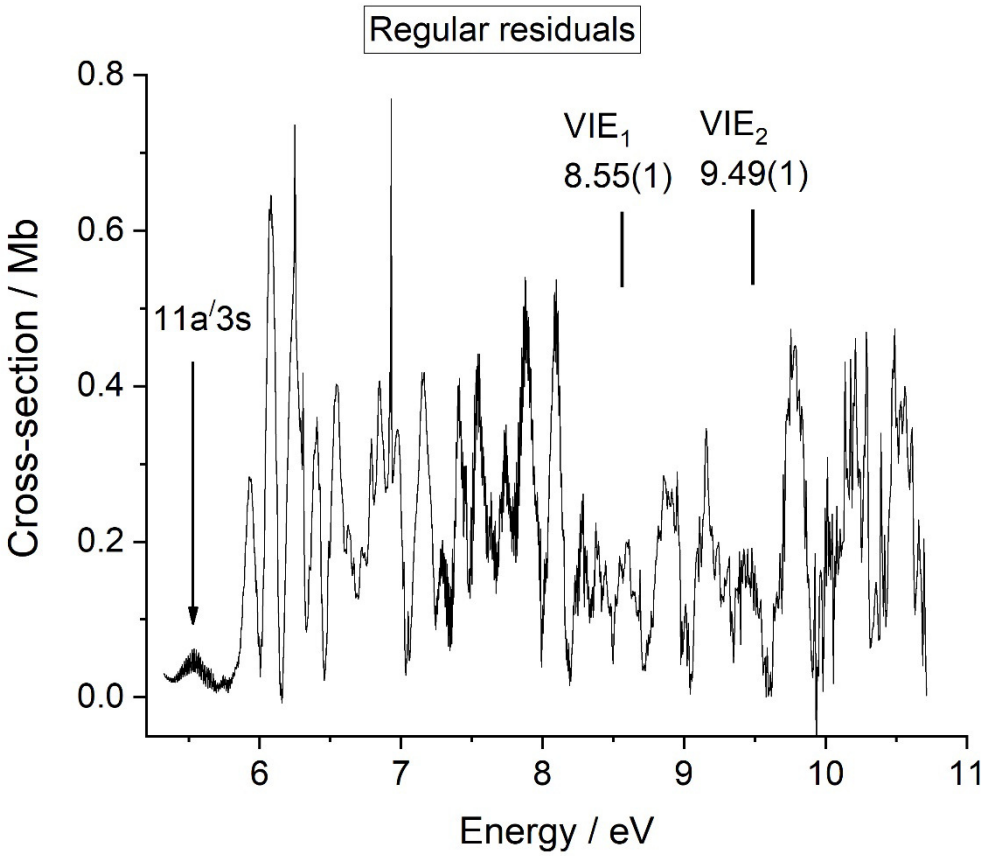
Regular residuals
VIE1
8.55(1)
VIE2
9.49(1)
11a′3s
Cross-section / Mb
0.0
0.2
0.4
0.6
0.8
6
7
8
9
10
11
Energy / eV